# Accepted Manuscript

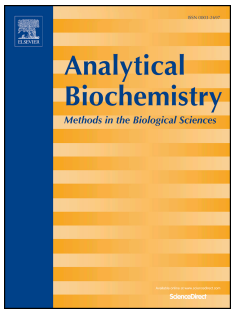


Electrochemical enzymatic fenitrothion sensor based on a tyrosinase/poly(2-hydroxybenzamide)-modified graphite electrode

Maria de Fátima Alves, Ricardo Augusto Moreira de Souza Corrêa, Filipe Soares da Cruz, Diego Leoni Franco, Lucas Franco Ferreira

PII: S0003-2697(18)30512-8

DOI: 10.1016/j.ab.2018.05.014

Reference: YABIO 13020

To appear in: *Analytical Biochemistry*

Received Date: 5 November 2017

Revised Date: 30 January 2018

Accepted Date: 15 May 2018

Please cite this article as: M. de Fátima Alves, R.A. Moreira de Souza Corrêa, F. Soares da Cruz, D.L. Franco, L.F. Ferreira, Electrochemical enzymatic fenitrothion sensor based on a tyrosinase/poly(2-hydroxybenzamide)-modified graphite electrode, *Analytical Biochemistry* (2018), doi: 10.1016/j.ab.2018.05.014.

# Electrochemical enzymatic fenitrothion sensor based on a tyrosinase/poly(2-hydroxybenzamide)-modified graphite electrode

Maria de Fátima Alves[a], Ricardo Augusto Moreira de Souza Corrêa[a], Filipe Soares da Cruz[a], Diego Leoni Franco[b] and Lucas Franco Ferreira[a*]

[a] Laboratório de Eletroquímica e Nanotecnologia Aplicada, Instituto de Ciência e Tecnologia, Universidade Federal dos Vales do Jequitinhonha e Mucuri, Rodovia MGT 367, Km 583, 5000, Alto da Jacuba, Diamantina-MG, 39100-000, Brazil.

[b] Grupo de Eletroquímica Aplicada a Polímeros e Sensores, Laboratório de Eletroanalítica Aplicada à Biotecnologia e Engenharia de Alimentos, Instituto de Química, Universidade Federal de Uberlândia, Campus Patos de Minas, Av. Getúlio Vargas, 230, Patos de Minas-MG, 38700-128, Brazil.

*** Corresponding author:**

E-mail: lucas.franco@ict.ufvjm.edu.br
Telephone: +55 (38) 3532-1214
ORCID: 0000-0002-5431-0069

**Abstract**

This paper reports the electrosynthesis and characterisation of a polymeric film derived from 2-hydroxybenzamide over a graphite electrode and its application as an enzymatic biosensor for the determination and quantification of the pesticide fenitrothion. The material was analysed by scanning electron microscopy and its electrochemical properties characterised by cyclic voltammetry and electrochemical impedance spectroscopy. The enzyme tyrosinase was immobilised over the modified electrode by the drop and dry technique. Catechol was determined by direct reduction of biocatalytically formed *o*-quinone by employing the flow injection analysis technique. The analytical characteristics of the proposed sensor were optimised as follows: phosphate buffer 0.050 M at pH 6.5, flow rate 5.0 mL $min^{-1}$, sample injection volume 150 µL, catechol concentration 1.0 mM and maximum inhibition time by fenitrothion of 6 min. The biosensors showed a linear response to pesticide concentration from 0.018 to 3.60 µM. The limit of detection and limit of quantification were calculated as 4.70 nM and 15.9 nM (RSD < 2.7%), respectively. The intra- and inter-electrode RSDs were 3.35% (n = 15) and 8.70% (n = 7), respectively. In addition, water samples spiked with the pesticide showed an average recovery of 97.6% (±1.53).

**Keywords:** 2-hydroxybenzamide; electropolymerization; catechol; biosensor; tyrosinase; fenitrothion.

## 1. Introduction

Since the prohibition of organochlorine pesticides due to their harmful effects on the environment, organophosphates have become the main pesticides used worldwide due to their good degradability, lower toxicity and low persistence in mammalian systems compared with organochlorines [1,2].

Among the available compounds, fenitrothion (*O*,*O*-dimethyl *O*-(3-methyl-4-nitrophenyl) phosphorothioate) is one of the most used organophosphate pesticides because it inhibits arthropod acetylcholinesterase (AChE) by oral and percutaneous routes of toxicity [3]. However, the indiscriminate use of these pesticides also causes contamination of soil, water and air. Due to its long range of dispersal in air, the pesticide can cause contamination of fauna and flora in places where it has not been spread [4]. This kind of contamination may also arise from other phenomena such as water eutrophication, groundwater contaminations [5] and an increased incidence of soil bacteria [6].

Although organophosphate contamination is less harmful than organochlorine, it may affect human health directly because the primary source of exposure is the ingestion of contaminated water and food [7]. Recent papers have shown that organophosphates may be linked to the development of several types of diabetes [8–10], neurotoxic effects [11], gestational hypertension [12], teratogenesis [13], genotoxicity [14] and carcinogenesis [15].

Therefore, the demand for novel methodologies or techniques to ensure food safety has stimulated research focused on food contaminated with pesticides, heavy metals and toxins [16]. In this respect, biosensors are a promising alternative in the search for an efficient technique to monitor contaminants in soil, water and food [17–24]. Some advantages include *in situ* analyses, low response time, high sensitivity and selectivity, low cost, the potential to be miniaturised and the lack of a requirement for highly skilled labour [25–26].

Among the several possibilities for biosensor construction, enzymatic devices with electrochemical detection have emerged as a promising alternative for pesticide detection [27–28], particularly acetylcholinesterase- [29–31] and tyrosinase (Tyr)-based sensors [32–34].

Tyr is responsible for the catalysis of *o*-phenol oxidation to *o*-quinones with efficiency in phenolic compound determination [35] (see equation 1). The electroactive

product can be determined and quantified through reduction using electrochemical techniques (equation 2). Tyr can be inhibited by pesticides such as carbamates, dithiocarbamates, chlorophenols and thioureas [36,37].

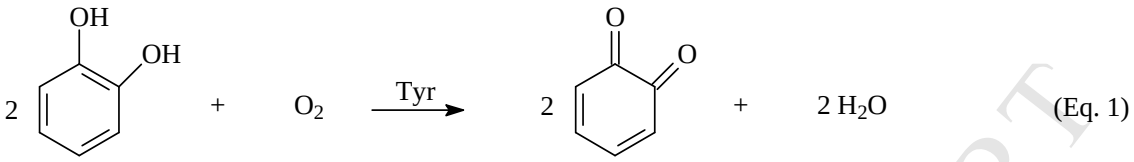


(Eq. 1)

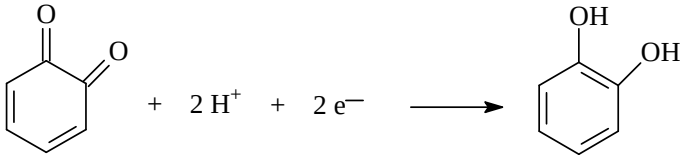


(Eq. 2)

Despite the many advantages of biosensors, the requirement for efficient enzyme immobilisation over the solid electrode surface to retain its activity is still a major challenge in their development [27]. It is necessary to preserve or improve protein stability, since these devices need to be stored for months and must therefore be robust [38]. In order to fulfil these requirements, intrinsically conducting polymers (ICPs) have been used due to their increased sensitivity and their ease of manufacture with the presence of functionalised groups, which form covalent bonds with the biomolecule [39].

The chemical compound 2-hydroxybenzamide (2-HBZ), also known as salicylamide, is a non-prescription drug with analgesic and antipyretic properties. Previous studies on electropolymerisation of aromatic compounds indicate that structures containing an oxygen atom bonded directly to an aromatic ring are easier to polymerise, and the film obtained presents high reproducibility and mechanical resistance, giving the modified electrode higher stability [40,41]. According to a recent study presented by da Cruz et al., the formation of a polymeric film derived from 2-HBZ over graphite electrodes may present conductivity as well as functional groups to bind directly with biomolecules [42].

Therefore, this work reports the development of an amperometric transducer based upon tyrosinase/poly(2-HBZ)-modified carbon graphite electrodes for the detection of the organophosphate pesticide fenitrothion in water samples. To the best of

our knowledge, this is the first study of 2-HBZ electropolymerisation and its use in biosensor development.

## 2. Experimental

### *2.1. Equipment and materials*

All electrochemical experiments were performed in a potentiostat/galvanostat from Autolab model PGSTAT 204, linked to a personal computer containing NOVA 1.10 software, where a Pt foil (A = 10 $mm^2$) was used as the counter electrode, while a Ag/AgCl (3.0 M KCl) electrode was used as the reference.

The flow injection analysis (FIA) system with amperometric detection was built with a four-channel peristaltic pump, Gilson model with Tygon tubes for fluid propulsion. The carrier solutions and samples were injected using a manual switch.

Tyrosinase from mushroom (EC. 1.14.18.1) (1.715 U $mg^{-1}$) and fenitrothion were obtained from Sigma-Aldrich (São Paulo, Brazil), catechol (99%) from Acros Organics (Geel, Belgica), 2-HBZ (99%) the graphite rod used as the working electrode (99.9995%) from Alfa Aesar (Ward Hill, USA), potassium ferrocyanide and potassium ferricyanide (99%) from Sigma-Aldrich (São Paulo, Brazil), perchloric acid (70%) from Vetec (Rio de Janeiro, Brazil) and sodium hydroxide (97%), potassium phosphate dibasic and monobasic (99%) from Reagen (Parana, Brazil).

### *2.2. Electropolymerisation of 2-hydroxybenzamide*

Firstly, the graphite electrode (GE) (A = 29.7 $mm^2$) was mechanically polished with alumina slurry (0.3 μm), ultrasonicated, washed with distilled water and dried in $N_2$ (g). Then, the electrodes were conditioned in solutions of the supporting electrolyte perchloric acid with 5% ethyl alcohol (3 cycles of potential scanning from +0.20 to +1.20 V) and subsequently in potassium ferrocyanide/ferricyanide solution (3 cycles of potential scanning from –0.25 to +0.80 V). This conditioning ensured that no contamination occurred in the solutions or over the electrode surface. The electropolymerisation of 2-HBZ was carried out using the cyclic voltammetry technique with 100 successive cycles of potential from +0.0 to +1.20 V and a scan rate of 50 mV

$s^{-1}$ using a monomer of 2-hydroxybenzamide (2.5 mM) prepared in 0.5 M perchloric acid solution containing 5.0% ethyl alcohol.

*2.3. Morphological and electrochemical characterisation of poly(2-hydroxybenzamide)*

After electropolymerization, the electrodes were washed with deionised water and dried under $N_2$ (g) flow. The GE modified with poly(2-HBZ), named poly(2-HBZ)/GE, was then subjected to 5 cycles of potential scanning, in the same range of electropolymerization, to remove the residual monomer. For the analysis of ion exchange properties, ferro/ferricyanide and supporting electrolyte solutions were used to evaluate the electroactivity of poly(2-HBZ).

The micrographs of GE and poly(2-HBZ)/GE were verified from the SEM images obtained using a model TM-3000 tabletop microscope from Hitachi. Images were obtained at 15 kV using the backscattered electrons detected in composed mode.

Electrochemical impedance spectra were obtained in 5.0 mM $K_4[Fe(CN)_6]/K_3[Fe(CN)_6]$ solution containing 0.1 M KCl. The frequency range investigated was from $10^4$ to $10^{-2}$ Hz with a sine wave excitation amplitude of 10 mV (p/p) in the open circuit potential (OCP) of the system. Measurements were performed in order to investigate and analyse the surface electrical properties of GE and poly(2-HBZ)/GE. Fitting of the impedance spectra to a model equivalent circuit was carried out using the Autolab PGSTAT 204 with NOVA 1.10 software.

*2.4. Construction and optimisation of the biosensor*

Tyr stock solution was prepared by dissolving 25,000 U (14.58 mg Tyr) in 4.0 mL phosphate buffer 0.05 M, pH 6.5. Then, 20 µL of the stock solution was diluted in 200 µL of phosphate buffer, and finally, 25 µL was dripped over the modified electrode (15.6 U), kept for 2 h at 37 °C in a drying oven, washed in buffer solution for 6 seconds with stirring and dried under $N_2$ (g) flow.

FIA was used to monitor the response of the sensor in the presence of the substrate catechol through electrochemical reduction of the enzymatic product *o*-quinone by chronoamperometry at −0.20 V. The following biosensor conditions were optimised: carrier solution (pH 5.0–8.0), volume of injected sample (50–300 µL),

electrolyte flow rate (1–8 mL $min^{-1}$), *o*-quinone reduction potential (−0.40–0.00 V), substrate concentration ($1.0 \times 10^{-6}$–$1.0 \times 10^{-2}$ M) and incubation time (0.5–10 min).

### *2.5. Analysis of fenitrothion*

For measurement of the biosensor inhibition rate by the insecticide fenitrothion, 1.0 mM catechol solution prepared in 0.05 M phosphate buffer (pH 6.5) was used as a substrate. The reduction current was measured after 6 min of contact of the biosensor with fenitrothion solutions at concentrations of 5–1000 ppb.

Tap water samples were collected directly from public systems and spiked with fenitrothion. The inhibition rate (%*I*) was measured as the decrease in reduction current of *o*-quinone calculated by equation 3:

$$(\%\, I) = \frac{\Delta I}{I_0} \times 100 \qquad \text{(Eq. 3)}$$

where $\Delta I$ is the difference between the current value of *o*-quinone reduction before and after addition of fenitrothion, and $I_o$ is the *o*-quinone reduction current value before addition of fenitrothion.

## 3. Results and discussion

### *3.1. Electrosynthesis of poly(2-HBZ)*

For film formation, 100 successive scans were carried out in a solution containing the monomer and the supporting electrolyte as shown in Figure 1.

INSERT FIGURE 1

The oxidation current peak near +1.07 V observed in Figure 1 was attributed to monomer oxidation. In the first reverse scan, cathodic processes at +0.75 and +0.50 V were observed and attributed to the reduction of adsorbed material over the electrode. In the subsequent scan it was confirmed by the appearance of three reversible redox peaks

(+0.75, +0.50 and +0.33 V for reduction and +0.95, +0.57 and +0.38 V for oxidation). A current increase at these redox peaks together with a current decrease at the more anodic oxidation peak ($I_{p,a}$) was observed with the subsequent scans. This behaviour suggests progressive monomer depletion over the electrode/solution interface and the formation and adsorption of an electroactive material over the graphite surface.

A detailed analysis of each wave in the CV presented in Figure 1 reveals rather high complexity. The positions of the amide and hydroxyl groups in the aromatic ring clearly indicate the high complexity of CV behaviour. The ortho position can cause an interaction between the oxygen atom from the hydroxyl group and the nitrogen atom from the amide group; therefore, different oxidizable and reducible species may be formed, resulting in the electroactivity observed for the polymeric film. However, a CV comparison was used to evaluate the electrochemical properties of the adsorbed polymeric film, as well as its role in the charge transfer process of the ferro/ferricyanide redox couple, as will be shown in section 3.3. Hence, through CV analysis, it will be possible to understand some electrochemical properties of poly(2-HBZ).

*3.2. Morphologic studies*

The morphology of GE and poly(2-HBZ)/GE were analysed by SEM, and the images are shown in Figure 2.

INSERT FIGURE 2

The micrographs show the morphological differences between the GE (Figure 2A) and the poly(2-HBZ)/GE (Figure 2B). As usual, the GE presents a surface with the presence of minor grooves throughout its extension, because of its high porosity. After electropolymerisation the electrode shows homogeneous coverage with a whisker-like material, covering even the graphite minor grooves. The different magnifications ensure the homogeneity of the polymer coverage over the electrode surface in comparison with the unmodified electrode.

*3.3. Electrochemical characterisation of poly(2-HBZ)*

The electrochemical behaviour of GE and poly(2-HBZ)/GE in solutions containing the supporting electrolyte (0.5 M $HClO_4$ + 5% absolute ethanol) and redox probe (5.0 mM $K_4Fe(CN)_6/K_3Fe(CN)_6$ containing 0.1 M KCl) is shown in Figure 3.

INSERT FIGURE 3

It is clear from the data in Figures 3A and 3B that the electrode surface was modified. The same redox peaks observed during electropolymerisation appear in the CVs containing only the supporting electrolyte, suggesting an electroactive material adsorbed over the GE (Fig. 3A). Figures 3B and 3C show the intrinsic electrochemical response exhibited by poly(2-HBZ) in the presence and absence of the redox probe (outer-sphere reaction). This strategy was used to avoid inadequate data analysis, eliminating the polymeric response by measuring the supporting electrolyte solution, leaving only the desired redox pair response. Therefore, the kinetics of electron transport at the solution/poly(2-HBZ) interface shown in Figure 3B suggest that for poly(2-HBZ)/GE the observed faradaic process is practically attributed to the electroactivity of the polymeric film in this medium (0.1 M KCl) as observed in Figure 3C, which shows a block in the redox activity of the ferro/ferricyanide couple on the surface of the electrode. It also shows that there is a current decrease ($I_{p,a}$ and $I_{p,c}$) compared to bare GE and a potential shift to more anodic potentials. This current decrease may reflect an increase in charge transfer resistance due to polymer deposition, interfering in the electrochemical response of the redox pair.

*3.4. Electrochemical impedance spectroscopy studies*

The electrochemical impedance spectroscopy (EIS) spectra obtained for GE and poly(2-HBZ)/GE in the presence of the redox probe (outer sphere redox reaction) were obtained at the open-circuit potential (OCP) and are shown in Figure 4.

INSERT FIGURE 4

It is known that the response in the frequency domain for an electrode process is characterised by a straight line in the diagram of a complex plane (-Z" *vs*. Z') with an inclination of 45° (Warburg line). Moreover, according to the EIS theory, a quasi-

reversible system is characterised by the presence of a semicircle connected to a linear segment with an inclination of 45° in the complex plane. As expected, this behaviour was found for the unmodified electrode (GE). In these systems the high frequency range is characterised by the solution properties, where the intercept with the real axis (Z') provides the non-compensated resistance value of the solutions, $R_s$. The impedimetric responses in the medium frequency range are associated with the interfacial processes between the electrode and solution. The relaxation phenomenon is observed in the Nyquist diagram, which is presented as a semicircle with constant time defined by the product of resistance to charge transfer $R_{ct}$ and the pseudocapacitance of the electric double layer $Q_{dl}$. In the lower frequency range, the impedance becomes controlled by the diffusion of the electroactive species with a representative response of mass transport in the complex plane characterised by a linear behaviour with an independent frequency phase angle of $\pi/4$.

On the other hand, the modified electrode presents a highly resistive behaviour resulting from the slow kinetics of the electronic transference reaction between the electroactive species in the solution and the redox sites of the polymer formed. In this case, electronic transport through the polymeric chain is followed by transport of the counterion. This ion movement can be compared to the charge/discharge of a capacitor. Since the polymeric chain "surface" presents irregular geometry, the double layer also presents a constant phase element (CPE) behaviour.

In order to obtain a quantitative treatment of EIS spectra, it is necessary to make use of a theoretical model that represents the physical properties of the electrode/solution interface. In this context, the theoretical model of Randles $R_s(Q_{dl}[R_{ct}W])$, describing the GE, is the most recommended to represent the behaviour of redox reactions of the outer sphere in the frequency domains. Electrode processes occur at the electrode/solution interface in the absence of kinetic complications due to the adsorption of electrolyte species or reaction intermediates as observed for the unmodified electrode. Moreover, for the poly(2-HBZ)/GE, a circuit of Ladder $R_s(Q_{dl}[R_{ct}(Q_fR_f)])$ represents the obtained spectra more appropriately. The $R_f$ element (the ionic transport resistance) and $Q_f$ element (pseudocapacitance) are associated with the charge/discharge process of the polymeric chain.

The apparent values of the equivalent circuits obtained from the numeric simulation based on the geometric area of the electrodes are summarised in Table 1.

INSERT TABLE 1

The $R_{ct}$ obtained in the OCP acts as an indirect measure of the exchange current density ($I_o = RT/nFR_{ct}$) for the redox reaction of the outer sphere at the electrode/solution interface. The approximate 5-fold increase of $R_{ct}$ in the modified electrode suggests that the presence of the polymer strongly affects the electronic transference kinetics of the redox pair $Fe(CN)_6^{3-}/Fe(CN)_6^{4-}$. Moreover, the approximately 4-fold increase in the value of $Q_{dl}$ [poly(2-HBZ) > GE] suggests that the modified electrode presents a more compact surface when compared with the graphite electrode, suggesting that the polymeric material grows in the inner grooves of the graphite and not on the external surface. This result corroborates the micrographs obtained through SEM. The linearity of the system was verified through the Kramers–Krönig transform method with values lower than $10^{-5}$, and all the data presented have good consistency since the $\chi^2$ remained in the order of $10^{-3}$.

*3.5. Performance and optimisation of the biosensor*

After confirmation of polymer formation, the Tyr enzyme was immobilised over the modified carbon electrode, and the chronoamperometry technique was used for *o*-quinone detection through the FIA system. The proposed biosensor is based upon the inhibition of Tyr by fenitrothion, decreasing the oxidation rate to *o*-quinone. The *o*-quinone produced in the reaction described by equation 1 can be monitored over the transducer through its electrochemical reduction (equation 2). Enzymatic inhibition by fenitrothion decreases the amount of *o*-quinone, and the signal difference is proportional to the inhibition and hence, to the pesticide. The applied potential and pH value for chronoamperometry were the first parameters to be optimised. Figure 5A presents the maximum current peaks of *o*-quinone reduction in a potential range from –0.40 to 0.00 V and Figure 5B in the pH range from 5.0 to 8.0. A representative FIA-gram is shown as an inset in Figure 5.

As observed in Figure 5A, the optimal applied potential with the highest current peak for *o*-quinone reduction was –0.20 V. An experiment performed through CV using a solution containing catechol resulted in oxidation to *o*-quinone and a subsequent reduction to catechol with a current peak exactly at this potential value. Thus, it was

expected that, using the chronoamperometry technique, the best potential would be –0.20 V (the higher the current response, the higher the analyte concentration). The supporting electrolyte as well the pH value must ensure enzyme stability without a loss of activity. Every enzyme presents an optimal pH, and variation in this parameter may decrease enzyme efficiency. As observed from Figure 5B, the carrier solution pH value directly affects the biosensor response, and the best result was obtained at a pH value of 6.5.

INSERT FIGURE 5

Figure 5C presents the flow rate study. It is observed that at values higher than 5.0 mL/min, current peak values reached a plateau. When the flow rate increased, the sample dispersion decreased. Therefore, the current value increased until it reached a maximum and from that point on did not change considerably. Also, at the beginning of the plateau, a lower cleaning time occurred beyond the minimisation of the lixiviation effect. Therefore, the flow rate was fixed at 5.0 mL $min^{-1}$.

The sampling loop was varied from 50 to 300 μL as observed from Figure 5D to evaluate the effect of the volume of substrate injected. The amperometric signal increased proportionally with the volume of substrate added because of the lower dispersion effect from the moment of injection to the moment the substrate reached the electrochemical detector. With more substrate, more products are formed, and consequently, a higher electrochemical signal is generated. Moreover, in the range of the sampling loop analysed, it was not possible to observe enzyme saturation, and the signal remained constant. As the current did not change significantly in the range analysed (10–11.5 μA) and to avoid the use of unnecessary amounts of substrate, a sampling loop volume of 150 μL was chosen. This is an intermediate value and presents a reasonable response.

In order to verify the reproducibility of the system, 15 catechol samples were injected using these optimised conditions (catechol concentration: 1.0 mM in phosphate buffer 0.050 M (pH 6.5), $E_{ap}$: –0.20 V, flow rate: 5.0 mL $min^{-1}$ and sampling loop: 150 μL), and the relative standard deviation (RSD) obtained was 3.35% (intra-electrode). The same analysis was performed for seven different biosensors prepared on different

days with the same concentration of catechol, resulting in an inter-electrode RSD value of 8.70%.

Figure 6 shows the biosensor linear range from the data on peak current obtained as a function of catechol concentration (inset).

A linear relationship is observed at catechol concentrations between $1.0 \times 10^{-5}$ and $1.0 \times 10^{-3}$ M with a sensitivity of 3.22 μA/mM and a linear correlation coefficient of $r^2 = 0.9988$. Above this concentration a peak current appears to reach a plateau, probably due to saturation of the enzyme's active site.

INSERT FIGURE 6

*3.6. Fenitrothion analysis*

Following parameter optimization, the biosensor was applied to detect the pesticide fenitrothion. The base signal ($\Delta I_0$) was measured in a solution containing only a fixed concentration of the substrate. Afterwards, the biosensor was taken to a second solution containing fenitrothion for Tyr inhibition. Then the system was again placed in the solution containing only catechol and the base signal measured ($\Delta I$). As this signal was proportional to the substrate concentration based on the electrochemical response of *o*-quinone, the decrease in enzymatic activity due to fenitrothion inhibition led to variation in the base signal.

The contact time of the biosensor with the pesticide in solution is an important factor in the determination of enzymatic inhibition. The %*I* calculated by equation (3) for the immobilised enzyme as a function of biosensor incubation time in a solution containing 1000 ppb of fenitrothion increased for the first 6 minutes of incubation (see Figure 7A), reaching 98% inhibition with no significant changes after this time. Therefore, this time was used for pesticide detection and quantification.

INSERT FIGURE 7

Figure 7B presents %*I* as a function of fenitrothion concentration ranging from 5 to 1000 ppb (0.018–3.6 μM) with a sensitivity of 0.075% inhibition/ppb. Inhibition followed a linear relationship in the studied range, with the limit of detection (LOD),

determined as three times the standard deviation of the signal for the buffer (blank), of 1.3 ppb (4.7 nM) of fenitrothion.

A comparison of the proposed biosensor with the other previously reported electrochemical sensors for fenitrothion analysis is shown in Table 2. Thus, poly(2-HBZ) is a very promising biosensor construct for fenitrothion determination based on tyrosinase inhibition. Considering that in Brazil there is no specific legislation defining the allowable limits of organophosphate pesticide concentration in water, the LOD obtained by the biosensor allows the device to be applied following the WHO guidelines that define the safety level of 8.0 ppb (28.8 nM) for fenitrothion in water samples [49].

INSERT TABLE 2

Water samples were spiked with 50 ppb of fenitrothion. Analyses were performed in triplicate, and an average recovery of 97.6% with a relative standard deviation of ±1.53 was observed. In this context, it can be confirmed that this enzymatic biosensor can efficiently detect fenitrothion in environmental samples. Different biosensors were used for the determination of fenitrothion, and one biosensor was evaluated on multiple days. In all studies, a RSD of less than 5.0% was obtained, with an average loss of response of 17% after 30 days of use (stored at 4 °C), proving that the proposed method had good reproducibility. The method can be used for direct determination of fenitrothion in natural water samples, with no need for preliminary reactions, and only a short time is required for the analysis.

## 4. Conclusions

Characterisation of the electrochemical platforms showed the formation of an active electrochemical material on the surface of the GE. Several parameters were investigated to optimise the response of the biosensor to the substrate using the FIA analysis system. Among these investigations, the best responses were obtained under the following conditions: 0.05 M phosphate buffer pH 6.5 as the transporter fluid, flow rate of 5.0 mL $min^{-1}$, sample volume of 150 µL, substrate concentration of 1.0 mM, and a potential of −0.20 V applied at the working electrode. The working linear range for fenitrothion was 0.018–3.60 µM (linear correlation coefficient $r^2$ = 0.9735). The

equation obtained from the linear regression was: % inhibition = 24.4 + 0.075 [fenitrothion/ppb]. The limit of detection (LOD = 3σ/S) and limit of quantification (LOQ = 10σ/S) were calculated as 1.3 ppb (4.7 nM) and 4.4 ppb (15.9 nM) (RSD < 2.7%), respectively. The reproducibility was evaluated. The intra- and inter-electrode RSDs were 3.35% (n = 15) and 8.70% (n = 7), respectively. The electrodes were stored at 4 °C for 30 days, and a 17% loss of response was observed. In addition, samples of water spiked with the insecticide, on the order of 50 ppb, presented an average recovery of 97.6% with a standard deviation of ±1.53. The enzyme biosensor GE/(2-HBZ) is a viable alternative for the determination and quantification of the insecticide fenitrothion in environmental samples, such as water, using amperometric detection based on the enzymatic inhibition process of the insecticide, by the enzyme tyrosinase in the oxidation reaction of the catechol substrate.

## Acknowledgements

The authors are grateful for financial support from Conselho Nacional de Desenvolvimento Científico e Tecnológico (CNPq) (Process: 458996/2014-9, 460799/2014-2) and Fundação de Amparo à Pesquisa do Estado de Minas Gerais (FAPEMIG) (Project: APQ-00131-11, APQ-00711-14). The authors wish to thank the LMMA sponsored by FAPEMIG (CEX-112-10) and SECTES/MG for their support. This work is a collaborative research project of the members of the Rede Mineira de Química (RQ-MG) supported by FAPEMIG (Project: CEX - RED-00010-14).

## References

[1] J. Qiu, G. Chen, H. Zhou, J. Xu, F. Wang, F. Zhu, G. Ouyang, *In vivo* tracing of organophosphorus pesticides in cabbage (*Brassica parachinensis*) and aloe (*Barbadensis*), Sci. Total Environ. 550 (2016) 1134–1140.

[2] J.N. Seiber, L.A. Kleinschmidt, Contributions of pesticide residue chemistry to improving food and environmental safety: past and present accomplishments and future challenges, J. Agric. Food Chem. 59 (2011) 7536–7543.

[3] S. Lavarías, C.F. García, Acute toxicity of organophosphate fenitrothion on biomarkers in prawn *Palaemonetes argentinus* (Crustacea: Palaemonidae), Environ. Monit. Assess. 187 (2015) 65.

[4] R.J. Letcher, J.O. Bustnes, R. Dietz, B.M. Jenssen, E.H. Jørgensen, C. Sonne, J. Verreault, M.M. Vijayan, G.W. Gabrielsen, Exposure and effects assessment of persistent organohalogen contaminants in arctic wildlife and fish, Sci. Total Environ. 408 (2010) 2995–3043.

[5] X.-N. Zhang, Q.-P. Guo, X.-X. Shen, S.-W. Yu, G.-Y. Qiu, Water quality, agriculture and food safety in China: current situation, trends, interdependencies, and management, J. Integr. Agric. 14 (2015) 2365–2379.

[6] H. Itoh, R. Navarro, K. Takeshita, K. Tago, M. Hayatsu, T. Hori, Y. Kikuchi, Bacterial population succession and adaptation affected by insecticide application and soil spraying history, Front. Microbiol. 5 (2014) 457.

[7] F.P. Carvalho, Pesticides, environment, and food safety, Food Energy Secur. 6 (2017) 48–60.

[8] G.D. Shapiro, L. Dodds, T.E. Arbuckle, J. Ashley-Martin, A.S. Ettinger, M. Fisher, S. Taback, M.F. Bouchard, P. Monnier, R. Dallaire, A.-S. Morisset, W. Fraser, Exposure to organophosphorus and organochlorine pesticides, perfluoroalkyl substances, and polychlorinated biphenyls in pregnancy and the association with impaired glucose tolerance and gestational diabetes mellitus: the MIREC study, Environ. Res. 147 (2016) 71–81.

[9] R. Rezg, B. Mornagui, S. El-Fazaa, N. Gharbi, Organophosphorus pesticides as food chain contaminants and type 2 diabetes: a review, Trends Food Sci. Technol. 21 (2010) 345–357.

[10] K.W. Taylor, R.F. Novak, H.A. Anderson, L.S. Birnbaum, C. Blystone, M. Devito, D. Jacobs, J. Köhrle, D.H. Lee, L. Rylander, A. Rignell-Hydbom, R. Tornero-Velez, M.E. Turyk, A.L. Boyles, K.A. Thayer, L. Lind, Evaluation of the association between persistent organic pollutants (POPs) and diabetes in epidemiological studies: a national toxicology program workshop review, Environ. Health Perspect. 121 (2013) 774–783.

[11] H.-X. Liu, C.-F. Liu, W.-H. Yang, Clinical study of continuous micropump infusion of atropine and pralidoxime chloride for treatment of severe acute organophosphorus insecticide poisoning, J. Chin. Med. Assoc. 78 (2015) 709–713.

[12] C. Ledda, M. Fiore, L. Santarelli, M. Bracci, G. Mascali, M.G. D'Agati, A. Busà, M. Ferrante, V. Rapisarda, Gestational hypertension and organophosphorus pesticide exposure: a cross-sectional study, BioMed. Res. Int. 2015 (2015) 1–5.

[13] J. Seifert, The structural requirements of organophosphorus insecticides (OPI) for reducing chicken embryo NAD+ content in OPI-induced teratogenesis in chickens, Pestic. Biochem. Physiol. 129 (2016) 43–48.

[14] F. Taghavian, G. Vaezi, M. Abdollahi, A.A. Malekirad, Comparative toxicological study between exposed and non-exposed farmers to organophosphorus pesticides, Cell J. 18 (2016) 89–96.

[15] A.A. Zayed, A.I. Ahmed, A.M.T. Khattab, A.A. Mekdad, A.G. AbdelAal, Paraoxonase 1 and cytochrome P450 polymorphisms in susceptibility to acute organophosphorus poisoning in Egyptians, Neurotoxicology 51 (2015) 20–26.

[16] S.A. Mansour, M.H. Belal, A.A.K. Abou-Arab, M.F. Gad, Monitoring of pesticides and heavy metals in cucumber fruits produced from different farming systems, Chemosphere. 75 (2009) 601–609.

[17] S. Khaledian, M. Nikkhah, M. Shams-bakhsh, S. Hoseinzadeh, A sensitive biosensor based on gold nanoparticles to detect *Ralstonia solanacearum* in soil, J. Gen. Plant. Pathol. 83 (2017) 231–239.

[18] S.-H. Yang, K.-C. Cheng, V.H.-C. Liao, A novel approach for rapidly and cost-effectively assessing toxicity of toxic metals in acidic water using an acidophilic iron-oxidizing biosensor, Chemosphere. 186 (2017) 446–452.

[19] Y. Zeng, Z. Zhu, D. Du, Y. Lin, Nanomaterial-based electrochemical biosensors for food safety, J. Electroanal. Chem. 781 (2016) 147–154.

[20] F.C. Vicentini, L.L.C. Garcia, L.C.S. Figueiredo-Filho, B.C. Janegitz, O. Fatibello-Filho, A biosensor based on gold nanoparticles, dihexadecylphosphate, and tyrosinase for the determination of catechol in natural water, Enzyme Microb. Technol. 84 (2016) 17–23.

[21] C. Durrieu, Y. Ferro, M. Perullini, A. Gosset, M. Jobbágy, S.A. Bilmes, Feasibility of using a translucid inorganic hydrogel to build a biosensor using immobilized algal cells, Environ. Sci. Pollut. Res. Int. 23 (2016) 9–13.

[22] J. Bao, C. Hou, M. Chen, J. Li, D. Huo, M. Yang, X. Luo, Y. Lei, Plant esterase–chitosan/gold nanoparticles–graphene nanosheet composite-based biosensor for the ultrasensitive detection of organophosphate pesticides, J. Agric. Food Chem. 63 (2015) 10319–10326.

[23] S. Feng, F. Gao, Z. Chen, E. Grant, D.D. Kitts, S. Wang, X. Lu, Determination of α-tocopherol in vegetable oils using a molecularly imprinted polymers–surface-

enhanced Raman spectroscopic biosensor, J. Agric. Food Chem. 61 (2013) 10467–10475.

[24] L. Li, J. Liang, W. Hong, Y. Zhao, S. Sun, X. Yang, A. Xu, H. Hang, L. Wu, S. Chen, Evolved bacterial biosensor for arsenite detection in environmental water, Environ. Sci. Technol. 49 (2015) 6149–6155.

[25] R. Wang, J. Lin, K. Lassiter, B. Srinivasan, L. Lin, H. Lu, S. Tung, B. Hargis, W. Bottje, L. Berghman, Y. Li, Evaluation study of a portable impedance biosensor for detection of avian influenza virus, J. Virol. Methods 178 (2011) 52–58.

[26] V. Perumal, U. Hashim. Advances in biosensors: principle, architecture and applications, J. Appl. Biomed. 12 (2014) 1–15.

[27] R.R. Dutta, P. Puzari, Amperometric biosensing of organophosphate and organocarbamate pesticides utilizing polypyrrole entrapped acetylcholinesterase electrode, Biosens. Bioelectron. 52 (2014) 166–172.

[28] W. Zhang, A.M. Asiri, D. Liu, D. Du, Y. Lin, Nanomaterial-based biosensors for environmental and biological monitoring of organophosphorus pesticides and nerve agents, TrAC Trends Anal. Chem. 54 (2014) 1–10.

[29] V. Dhull, A. Gahlaut, N. Dilbaghi, V. Hooda, Acetylcholinesterase biosensors for electrochemical detection of organophosphorus compounds: A review, Biochem. Res. Int. 2013 (2013) doi: 10.1155/2013/731501.

[30] C.S. Pundir, N. Chauhan, Acetylcholinesterase inhibition-based biosensors for pesticide determination: a review, Anal. Biochem. 429 (2012) 19–31.

[31] M. Pohanka, Electrochemical biosensors based on acetylcholinesterase and butyrylcholinesterase. A review, Int. J. Electrochem. Sci. 11 (2016) 7440–7452.

[32] J.C. Vidal, S. Esteban, J. Gil, J.R. Castillo, A comparative study of immobilization methods of a tyrosinase enzyme on electrodes and their application to the detection of dichlorvos organophosphorus insecticide, Talanta 68 (2006) 791–799.

[33] P. Önnerfjord, J. Emnéus, G. Marko-Varga, L. Gorton, F. Ortega, E. Domínguez, Tyrosinase graphite-epoxy based composite electrodes for detection of phenols, Biosens. Bioelectron. 10 (1995) 607–619.

[34] F. Fartas, J. Abdullah, N. Yusof, Y. Sulaiman, M. Saiman, Biosensor based on tyrosinase immobilized on graphene-decorated gold nanoparticle/chitosan for phenolic detection in aqueous, Sensors 17 (2017) doi: 10.3390/s17051132.

[35] A. Sánchez-Ferrer, J.N. Rodríguez-López, F. García-Cánovas, F. García-Carmona, Tyrosinase: a comprehensive review of its mechanism, Biochim. Biophys. Acta. 1247 (1995) 1–11.

[36] Y.D.T. de Albuquerque, L.F. Ferreira, Amperometric biosensing of carbamate and organophosphate pesticides utilizing screen-printed tyrosinase-modified electrodes, Anal. Chim. Acta. 596 (2007) 210–221.

[37] J.S. Van Dyk, B. Pletschke, Review on the use of enzymes for the detection of organochlorine, organophosphate and carbamate pesticides in the environment, Chemosphere 82 (2011) 291–307.

[38] G.F. Grawe, T.R. de Oliveira, E. de Andrade Narciso, S.K. Moccelini, A.J. Terezo, M.A. Soares, M. Castilho, Electrochemical biosensor for carbofuran pesticide based on esterases from *Eupenicillium shearii FREI-39* endophytic fungus, Biosens. Bioelectron. 63 (2015) 407–413.

[39] S. Tuncagil, C. Ozdemir, D.O. Demirkol, S. Timur, L. Toppare, Gold nanoparticle modified conducting polymer of 4-(2,5-di(thiophen-2-yl)-1H-pyrrole-1-l) benzenamine for potential use as a biosensing material, Food Chem. 127 (2011) 1317–1322.

[40] R.C.Z. Lofrano, J.M. Madurro, L.M. Abrantes, J.R. Romero, Electrocatalytic hydrogenation of carbonylic compounds using an electrode with platinum particles dispersed in films of poly-[allyl ether *p*-(2-aminoethyl) phenol] co-polymerized with allyl phenyl ether, J. Mol. Catal. A Chem. 128 (2004) 73–79.

[41] R.C.Z. Lofrano, J.M. Madurro, J.R. Romero, Preparation and properties of an electrode coated with a cerium poly(allyl ether *p*-benzenesulfonate) film for electroorganic reactions, J. Mol. Catal. A Chem. 153 (2000) 237–242.

[42] F.S. da Cruz, F. de Souza Paula, D.L. Franco, W.T.P. dos Santos, L.F. Ferreira, Electrochemical detection of uric acid using graphite screen-printed electrodes modified with Prussian blue/poly(4-aminosalicylic acid)/uricase, J. Electroanal. Chem. 806 (2017) 172–179.

[43] Y. Lei, P. Mulchandani, W. Chen, A. Mulchandani, Biosensor for direct determination of fenitrothion and EPN using recombinant *Pseudomonas putida* JS444 with surface-expressed organophosphorus hydrolase. 1. Modified Clark Oxygen Electrode, Sensors 6 (2006) 466–472.

[44] Y. Lei, P. Mulchandani, W. Chen, A. Mulchandani, Biosensor for direct determination of fenitrothion and EPN using recombinant *Pseudomonas putida*

JS444 with surface-expressed organophosphorous hydrolase. 2. Modified carbon paste electrode, Appl. Biochem. Biotechnol. 136 (2007) 243–250.

[45] G. Bolat, S. Abaci, T. Vural, B. Bozdogan, E.B. Denkbas, Sensitive electrochemical detection of fenitrothion pesticide based on self-assembled peptide-nanotubes modified disposable pencil graphite electrode, J. Electroanal. Chem. 809 (2018) 88–95.

[46] L. Zhao, F. Zhao, B. Zeng, Synthesis of water-compatible surface-imprinted polymer via click chemistry and RAFT precipitation polymerization for highly selective and sensitive electrochemical assay of fenitrothion, Biosens. Bioelectron. 62 (2014) 19–24.

[47] O. Surucu, G. Bolat, S. Abaci, Electrochemical behavior and voltammetric detection of fenitrothion based on a pencil graphite electrode modified with reduced graphene oxide (RGO)/poly(E)-1-(4-((4-(phenylamino)phenyl)diazenyl)phenyl)ethanone (DPA) composite film, Talanta. 168 (2017) 113–120.

[48] A.A. Ensafi, R. Noroozi, N. Zandi-Atashbar, B. Rezaei, Cerium(IV) oxide decorated on reduced graphene oxide, a selective and sensitive electrochemical sensor for fenitrothion determination, Sens. Actuators B: Chem. 245 (2017) 980–987.

[49] WHO. World Health Organization: Chemical hazards in drinking-water: Fenitrothion. http://www.who.int/water_sanitation_health/water-quality/guidelines/chemicals/fenitrothion/en/, 2004 (accessed 11 January 2018).

**Figure Captions**

**Fig. 1.** Cyclic voltammograms of the GE in solutions containing 2.5 mM of 2-HBZ. Supporting electrolyte: 0.5 M $HClO_4$ + 5.0% absolute ethanol, 100 scans, $v$ = 50 mV $s^{-1}$. (- - -) First scan. The arrows signify the current direction.

**Fig. 2.** SEM images obtained for (A) GE and (B) poly(2-HBZ)/GE. Magnification of ×250 (A1 and B1) and ×1000 (A2 and B2).

**Fig. 3.** Cyclic voltammograms of (---) GE and (—) poly(2-HBZ)/GE in solutions containing (A) 0.50 M $HClO_4$ + 5.0% absolute ethanol; and (B) 5.0 mM $K_4Fe(CN)_6/K_3Fe(CN)_6$ + 0.1 M KCl and (C) 0.1 M KCl. $v$ = 100 mV $s^{-1}$.

**Fig. 4.** (A) Nyquist and (B) Bode diagrams for EIS spectra for (○) GE and (□) poly(2-HBZ)/GE. Electrolyte: 5.0 mM $K_4Fe(CN)_6/K_3Fe(CN)_6$ + 0.1 M KCl. Conditions for the impedance study: E = OCP; $\Delta E$ = 10 mV (RMS); and frequency range: $10^4$ to $10^{-2}$ Hz. The inset shows the equivalent circuit used in the simulation/fitting procedure. Solid lines represent the fit of the equivalent circuit to the experimental findings.

**Fig. 5.** Optimisation of biosensor. (A) Variation of $I_{p,c}$ *vs.* $E_{ap}$. Sampling loop: 150 µL, catechol concentration: 1.0 mM, phosphate buffer 0.050 M (pH 6.5) and flow rate: 5.0 mL $min^{-1}$; (B) Variation of $I_{p,c}$ at –0.20 V *vs*. pH value of phosphate buffer solution 0.050 M. Sampling loop: 150 µL, catechol concentration: 1.0 mM and flow rate: 5.0 mL $min^{-1}$; (C) Variation of $I_{p,c}$ *vs.* flow rate. $E_{app}$: –0.20 V, sampling loop: 150 µL, catechol concentration: 1.0 mM and phosphate buffer 0.050 M (pH 6.5) and (D) Variation of $I_{p,c}$ *vs.* sampling loop. $E_{ap}$: –0.20 V, catechol concentration: 1.0 mM, phosphate buffer 0.050 M (pH 6.5) and flow rate: 5.0 mL $min^{-1}$. Inset: FIA-gram.

**Fig. 6.** Linear response of amperometric biosensor. $E_{ap}$ = –0.20 V, sampling loop: 150 µL, flow rate: 5.0 mL $min^{-1}$, phosphate buffer solution 0.05 M, pH 6.5. Inset: Biosensor response evaluation *vs.* catechol concentration in the range $1.0 \times 10^{-5}$ to $1.0 \times 10^{-2}$ M.

**Fig. 7.** (A) Percentage of inhibition of the enzymatic biosensor *vs.* incubation time and (B) analytical curve obtained for detection and quantification of fenitrothion. $E_{ap}$ = –0.20 V, sampling loop: 150 µL, flow rate: 5.0 mL $min^{-1}$, catechol concentration: 1.0 mM, phosphate buffer solution 0.05 M, pH 6.5, [fenitrothion] = 5 to 1000 ppb.

**Table Captions**

**Table 1:** Apparent values of the equivalent circuit obtained in the numeric simulation using complex nonlinear least squares (CNLS) method.

**Table 2:** Comparison of some of the types of reported electrochemical sensors as a function of their performance for fenitrothion analysis.

**Table 1:** Apparent values of the equivalent circuit obtained in the numeric simulation using complex nonlinear least squares (CNLS) method.

| Parameter | GE | poly(2-HBZ)/GE |
|---|---|---|
| $R_s$ / Ω $cm^2$ | 42.4 | 43.1 |
| $R_{ct}$ / Ω $cm^2$ | 27 | 138 |
| $Q_{dl}$ /μΩ$^{-1}$cm$^{-2}$s$^n$ | 285 | 1100 |
| $n_{dl}$ | 0.7 | 0.5 |
| $Q_d$ /mΩ$^{-1}$cm$^{-2}$s$^n$ | 7.1 | --- |
| $n_d$ | 0.5 | --- |
| $R_f$/kΩ $cm^2$ | --- | 12.9 |
| $Q_f$/mΩ$^{-1}$cm$^{-2}$s$^n$ | --- | 6.3 |
| $n_f$ | --- | 0.8 |
| $\chi^2$ (x10$^{-3}$) | 1.2 | 45 |

**Table 2:** Comparison of some of the types of reported electrochemical sensors as a function of their performance for fenitrothion analysis.

| System | Surface electrode | Linear range (μM) | Limit of detection (nM) | Ref. |
|---|---|---|---|---|
| Microbial biosensor | Modified Clark Oxygen Electrode | up to 50 | 999 | 43 |
| Microbial biosensor | Modified Carbon Paste Electrode | up to 5.00 | 5.01 | 44 |
| Electrochemical | Peptide Nanotubes / Pencil Graphite Electrode | 0.114 - 1.712 | 19.6 | 45 |
| Electrochemical | Ionic Liquid Functionalized Graphene Coated Glassy Carbon | 0.01 – 5.00 | 8.00 | 46 |
| Electrochemical | Reduced Graphene Oxide / poly(E)-1-(4-((4-(phenylamino)phenyl)diazenyl)phenyl)ethanone / Pencil Graphite Electrodes | 0.10 – 1.91 | 3.48 | 47 |
| Electrochemical | $CeO_2$ Nanocomposite / GrapheneModified Glassy Carbon Electrode | 0.025 –2.00 | 3.00 | 48 |
| Enzymatic biosensor | Tyrosinase / poly(2-hydroxybenzamide) / Graphite Electrode | 0.018 - 3.6 | 4.70 | This work |

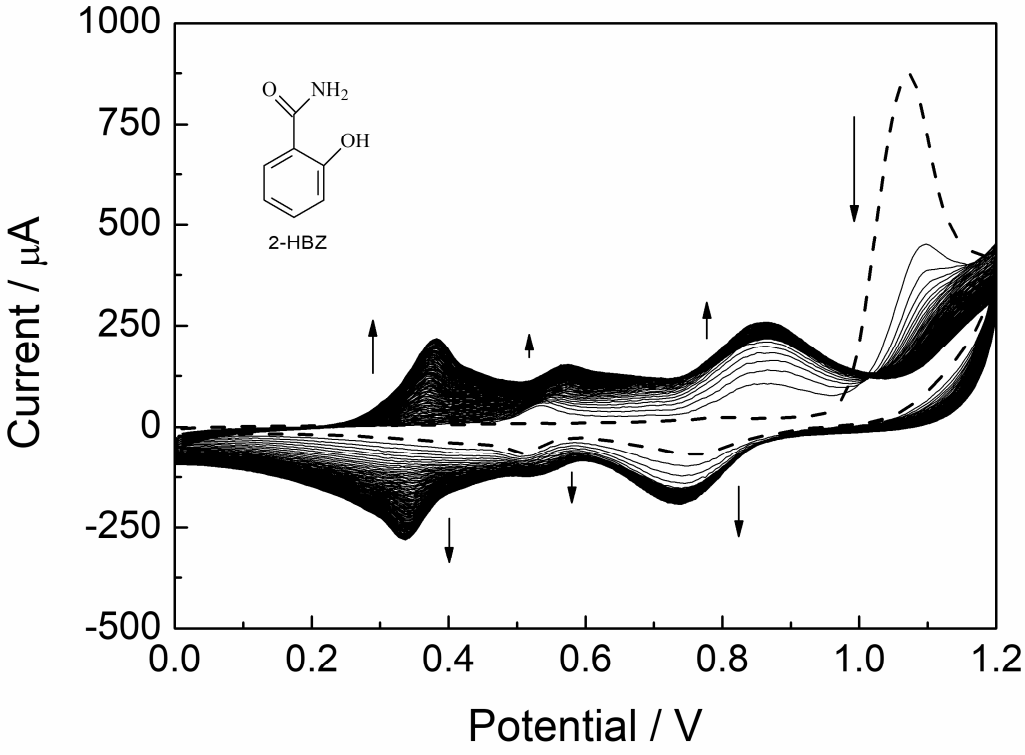

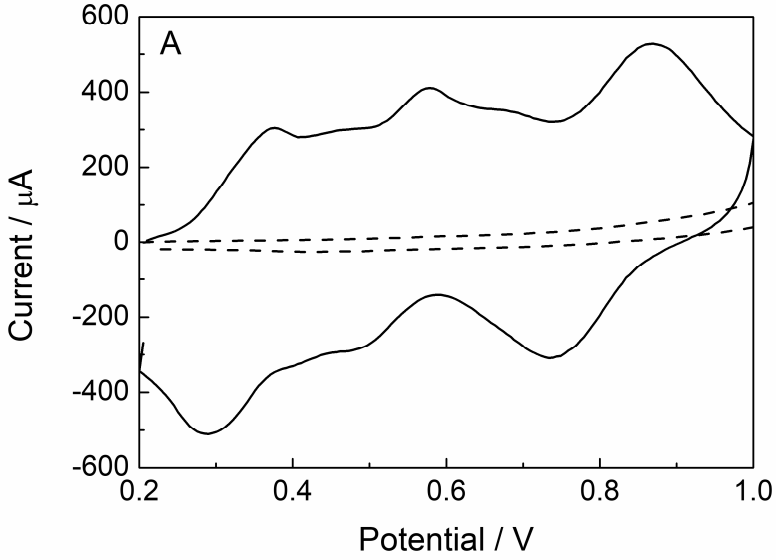
A
600
400
200
0
-200
-400
-600
0.2
0.4
0.6
0.8
1.0
Current / μA
Potential / V

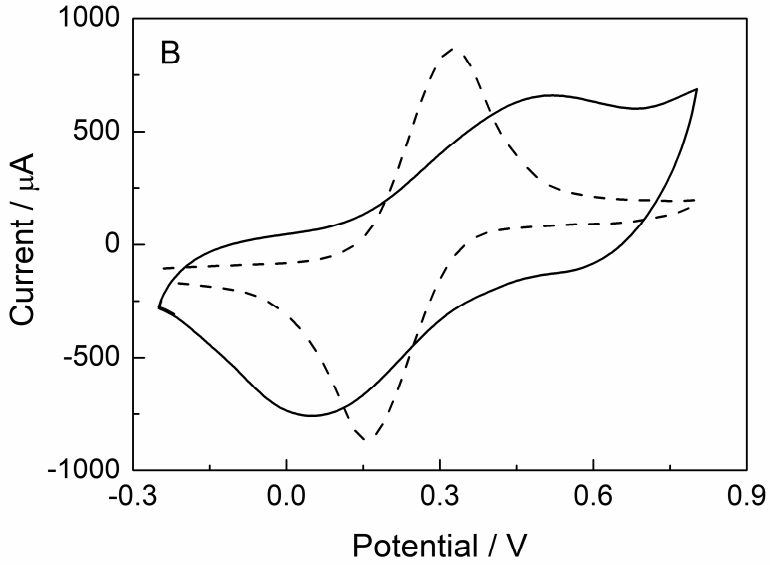
B
1000
500
0
-500
-1000
-0.3
0.0
0.3
0.6
0.9
Current / μA
Potential / V

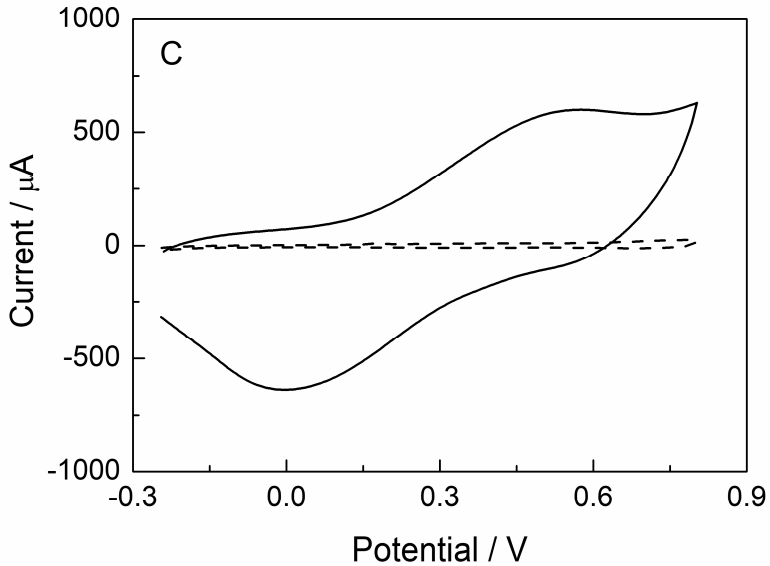
C
1000
500
0
-500
-1000
-0.3
0.0
0.3
0.6
0.9
Current / μA
Potential / V

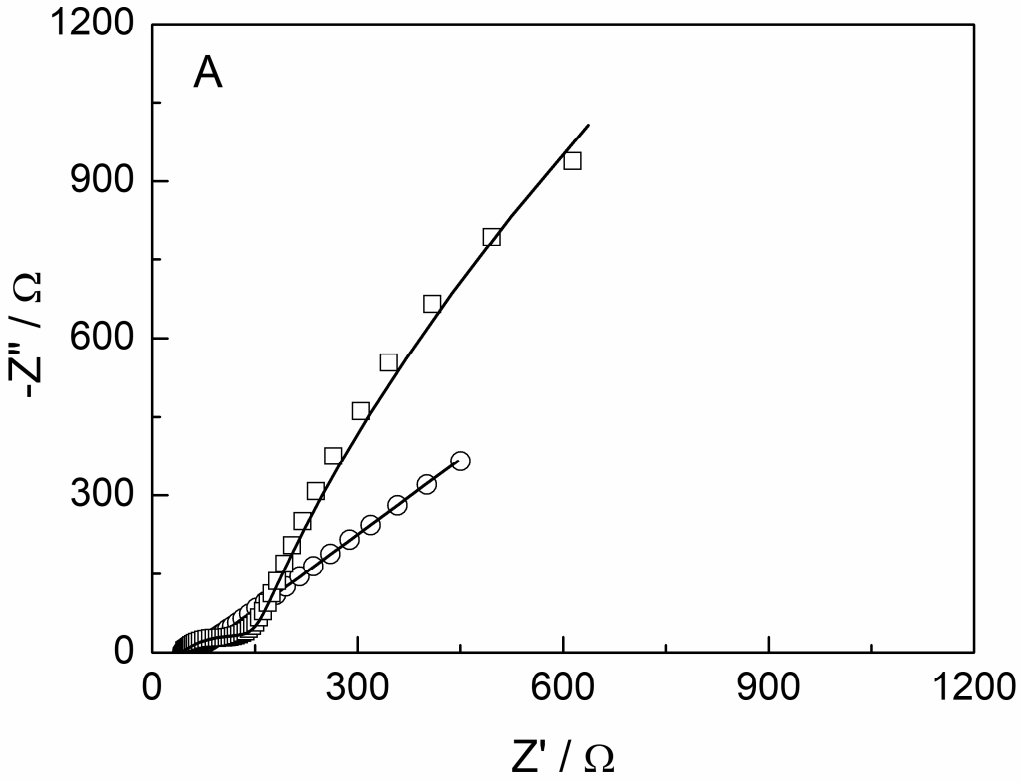
A
1200
900
600
300
0
-Z'' / Ω
0
300
600
900
1200
Z' / Ω

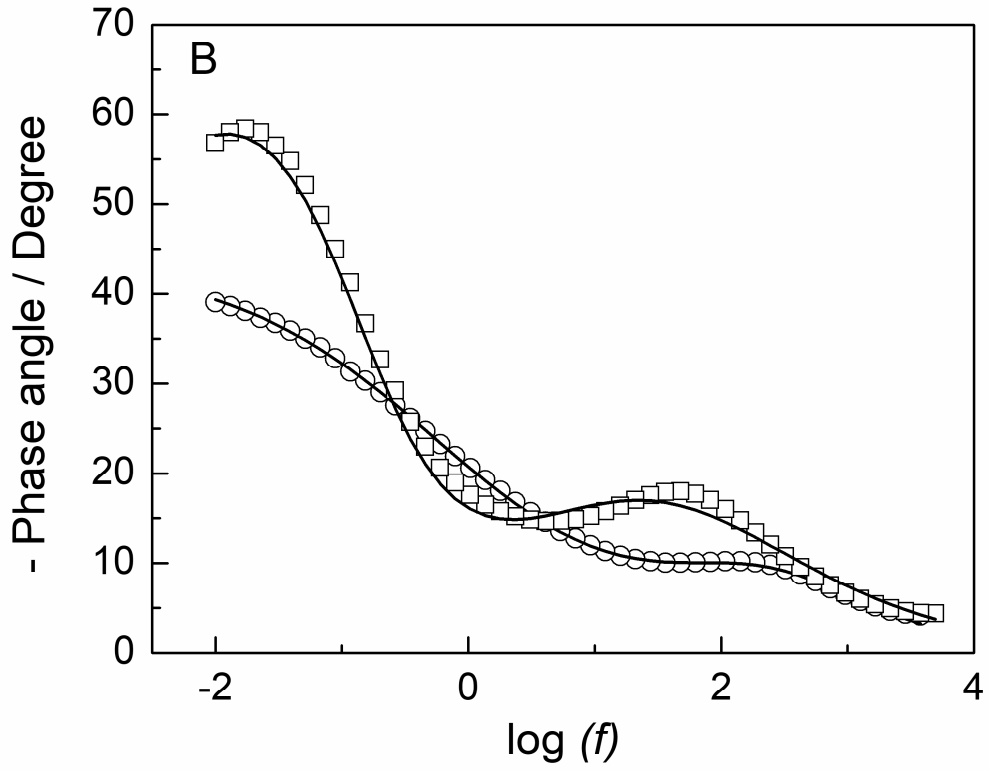
B
70
60
50
40
30
20
10
0
- Phase angle / Degree
-2
0
2
4
log (f)

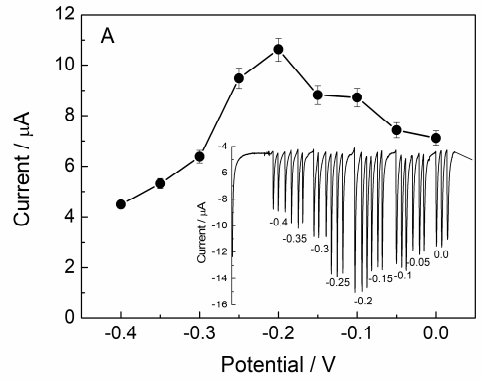


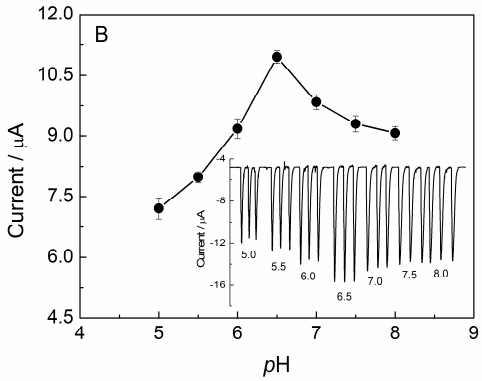


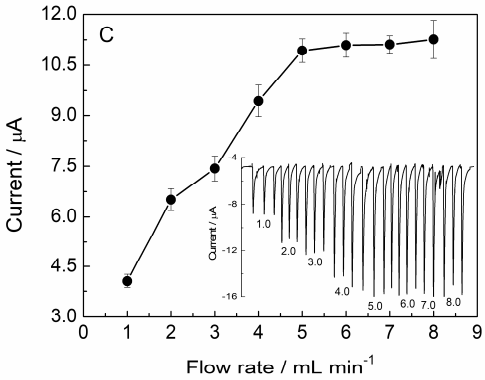


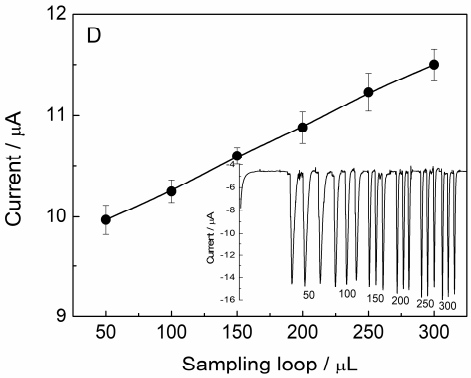

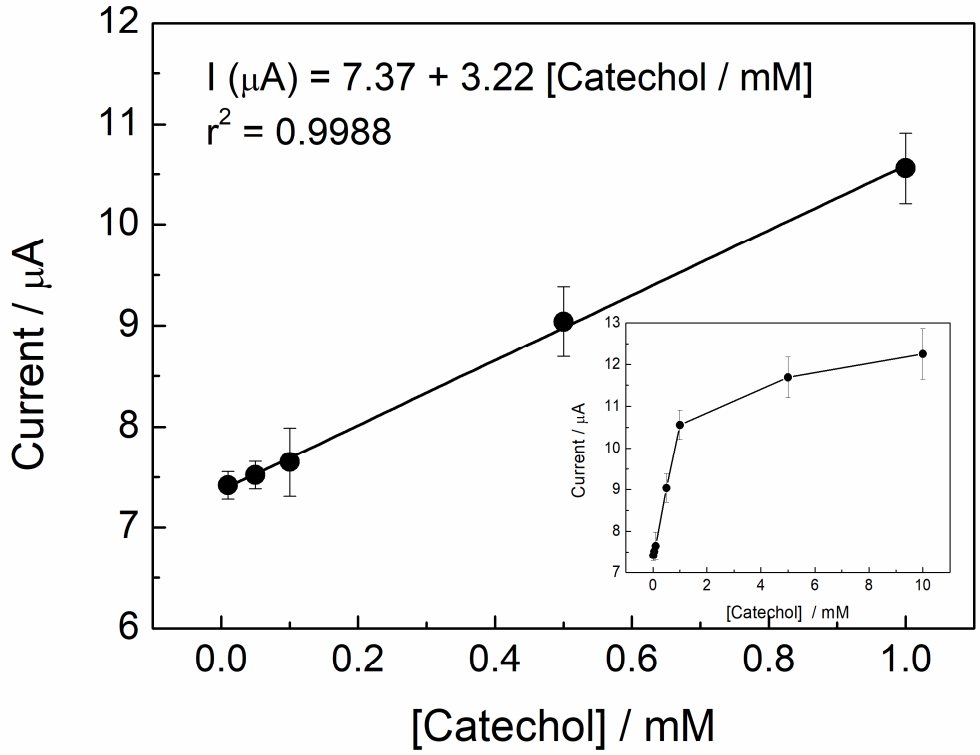

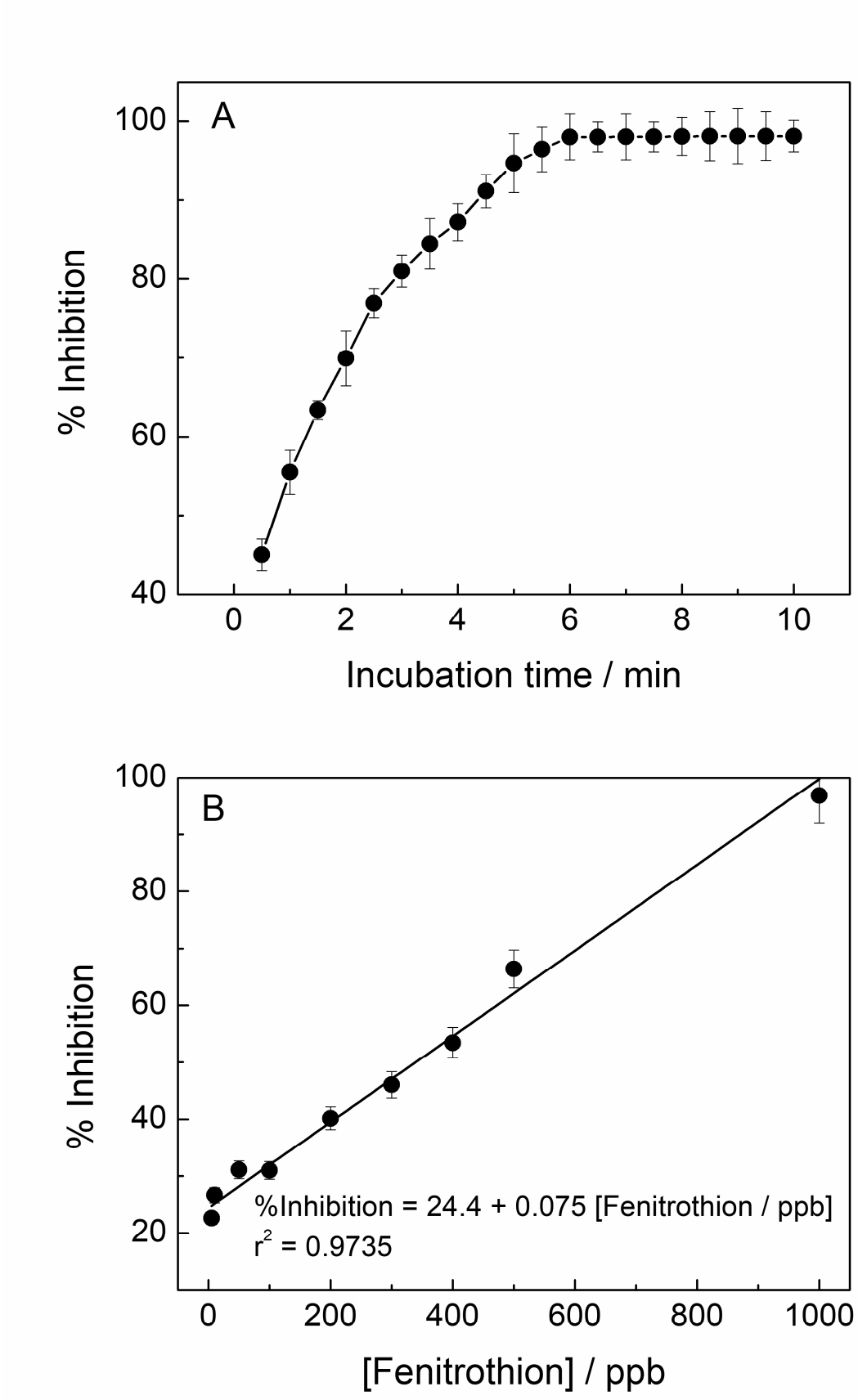
A
100
80
60
40
% Inhibition
0
2
4
6
8
10
Incubation time / min
B
100
80
60
40
20
% Inhibition
%Inhibition = 24.4 + 0.075 [Fenitrothion / ppb]
r2 = 0.9735
0
200
400
600
800
1000
[Fenitrothion] / ppb